



Chinese Society of Aeronautics and Astronautics  
& Beihang University  
**Chinese Journal of Aeronautics**

cja@buaa.edu.cn  
www.sciencedirect.com



# Closed-loop dynamic control allocation for aircraft with multiple actuators

Gai Wendong, Wang Honglun \*

Science and Technology on Aircraft Control Laboratory, Beihang University, Beijing 100191, China

Received 22 December 2011; revised 6 March 2012; accepted 2 July 2012  
Available online 30 April 2013

## KEYWORDS

Canard rotor/wing aircraft;  
Closed-loop control allocation;  
Dynamic inversion;  
Flight control systems;  
Redundant actuators

**Abstract** A closed-loop control allocation method is proposed for a class of aircraft with multiple actuators. Nonlinear dynamic inversion is used to design the baseline attitude controller and derive the desired moment increment. And a feedback loop for the moment increment produced by the deflections of actuators is added to the angular rate loop, then the error between the desired and actual moment increment is the input of the dynamic control allocation. Subsequently, the stability of the closed-loop dynamic control allocation system is analyzed in detail. Especially, the closed-loop system stability is also analyzed in the presence of two types of actuator failures: loss of effectiveness and lock-in-place actuator failures, where a fault detection subsystem to identify the actuator failures is absent. Finally, the proposed method is applied to a canard rotor/wing (CRW) aircraft model in fixed-wing mode, which has multiple actuators for flight control. The nonlinear simulation demonstrates that this method can guarantee the stability and tracking performance whether the actuators are healthy or fail.

© 2013 Production and hosting by Elsevier Ltd. on behalf of CSAA & BUAA.  
Open access under [CC BY-NC-ND license](#).

## 1. Introduction

Modern aircraft, automotive vehicles and marine vessels are usually equipped with more control actuators than controlled variables to achieve multiple control objectives and high performance. And the nonlinear control design methods, like dynamic inversion<sup>1,2</sup> and backstepping,<sup>3,4</sup> result in control laws specifying the forces and moments, rather than the control surface deflections. Determining how to distribute the control sig-

nals to the available actuators is known as the control allocation problem. Meanwhile, the actuator selection is separated from the regulation task to simplify the control design using the control allocation. In particular, an effective re-allocation among the remaining healthy actuators can maintain the acceptable performance in the case of actuator failures.

Control allocation methods have been studied extensively. The survey paper that compares the strengths and limitations of control allocation methods is presented in Ref.<sup>5</sup>. Regardless of methods, such as pseudoinverse,<sup>6</sup> direct allocation,<sup>7,8</sup> daisy chain allocation,<sup>9</sup> linear programming<sup>10</sup> and nonlinear programming,<sup>11</sup> the resulting methods are static in the sense that the control input depends only on the current virtual control command.

Different from these methods, the dynamic control allocation method<sup>12,13</sup> is proposed to make use of the redundancy to get different actuators operate in the different parts of frequency domain. The control allocation mapping of this method is a linear filter when there are no actuators in satura-

\* Corresponding author. Tel.: +86 10 82317546.

E-mail addresses: [gaiwd2011@gmail.com](mailto:gaiwd2011@gmail.com) (W. Gai), [hl\\_wang\\_2002@126.com](mailto:hl_wang_2002@126.com) (H. Wang).

Peer review under responsibility of Editorial Committee of CJA.



Production and hosting by Elsevier

tion state. And the control designer can decide the frequency characteristic of this filter by weighting matrices selected.

Both the static and the dynamic methods mentioned above are the open-loop control allocation. These control allocation approaches can be implemented to satisfy the optimization criterion when there is no actuator failure. However, the system stability or tracking performance becomes a problem if some unknown actuator failures occur.

Recently, a new nonlinear flight control design method is presented in Ref.<sup>14</sup> for aircraft with redundant actuators, combining the bases sequence control allocation with the moment compensation to implement the desired moment commands. However, this method fails to consider the closed-loop stability of control allocation system whether the actuators are healthy or fail. In this paper, a new systematic method for closed-loop dynamic control allocation is proposed, and the design process and stability analysis are introduced in detail.

## 2. Closed-loop dynamic control allocation

As mentioned in the first section, the control allocation plays an important role in nonlinear flight control for aircraft with multiple actuators, particularly, when the actuators have dynamics, limits and failures. A conceptual block diagram of the attitude control loop with closed-loop dynamic control allocation is shown in Fig. 1. The moments  $\mathbf{M}$  acting on the aircraft are given as

$$\mathbf{M} = \mathbf{M}_0 + \Delta\mathbf{M} \quad (1)$$

where  $\mathbf{M}_0$  is determined by the aircraft configuration and flight states, and  $\Delta\mathbf{M}$  the moment increments produced by the control surface deflections.

The control allocation problem is solved by the moment allocation among different actuators in this research. In Fig. 1, the input of system is the commanded attitude  $r_g$ . And the desired moment increment  $\Delta\mathbf{M}_d$  is derived by the nonlinear dynamic inversion attitude controller in outer-loop, while the actual moment increment  $\Delta\mathbf{M}$  can be measured by the angular acceleration sensors. Then, the error  $\mathbf{v}$  between the desired moment increments  $\Delta\mathbf{M}_d$  and the actual moment

increments  $\Delta\mathbf{M}$  is as the input of dynamic control allocation. Thus, the output of control allocation  $\mathbf{u}_v$  has the form of increment and one integration step delay is required. At last, the input of actuator is  $\mathbf{u}(k) = \mathbf{u}(k-1) + \mathbf{u}_v(k)$ , and  $k$  denotes the current sampling period. And the output of actuator  $\delta$  is deflections of actuators, which produces the actual moment increments  $\Delta\mathbf{M}$  and aerodynamic force  $\mathbf{F}$ .

### 2.1. Aircraft model

The aircraft model is described as<sup>15</sup>

$$\begin{cases} \dot{p} = (c_1 r + c_2 p)q + c_3 M_x + c_4 M_z \\ \dot{q} = c_5 p r - c_6(p^2 - r^2) + c_7 M_y \\ \dot{r} = (c_8 p - c_2 r)q + c_4 M_x + c_9 N_z \end{cases} \quad (2)$$

$$\begin{cases} \dot{V}_x = rV_y - qV_z - g \sin \theta + F_x/m \\ \dot{V}_y = -rV_x + pV_z + g \sin \phi \cos \theta + F_y/m \\ \dot{V}_z = qV_x - pV_y + g \cos \phi \cos \theta + F_z/m \end{cases} \quad (3)$$

$$\begin{cases} \dot{\phi} = p + (r \cos \phi + q \sin \phi) \tan \theta \\ \dot{\theta} = q \cos \phi - r \sin \phi \\ \dot{\psi} = (r \cos \phi + q \sin \phi) / \cos \theta \end{cases} \quad (4)$$

$$\begin{cases} \dot{x}_g = V_x \cos \theta \cos \psi + V_y (\sin \phi \sin \theta \cos \psi - \cos \phi \sin \psi) \\ \quad + V_z (\sin \phi \sin \psi + \cos \phi \sin \theta \cos \psi) \\ \dot{y}_g = V_x \cos \theta \sin \psi + V_y (\sin \phi \sin \theta \sin \psi + \cos \phi \cos \psi) \\ \quad + V_z (-\sin \phi \cos \psi + \cos \phi \sin \theta \sin \psi) \\ \dot{h} = V_x \sin \theta - V_y \sin \phi \cos \theta - V_z \cos \phi \cos \theta \end{cases} \quad (5)$$

where  $p$ ,  $q$  and  $r$  are the roll, pitch, and yaw angular rates;  $V_x$ ,  $V_y$  and  $V_z$  the components of flight velocity along the body axes;  $\phi$ ,  $\theta$  and  $\psi$  the roll, pitch, and yaw attitude angles;  $x_g$ ,  $y_g$  and  $h$  are respectively the north, east, and vertical components of the aircraft position in the locally-level geographic frame on the surface of the Earth;  $m$  is the mass of the aircraft, and  $g$  the gravity acceleration; the constants  $c_i$  ( $i = 1, 2, \dots, 9$ ) are defined by

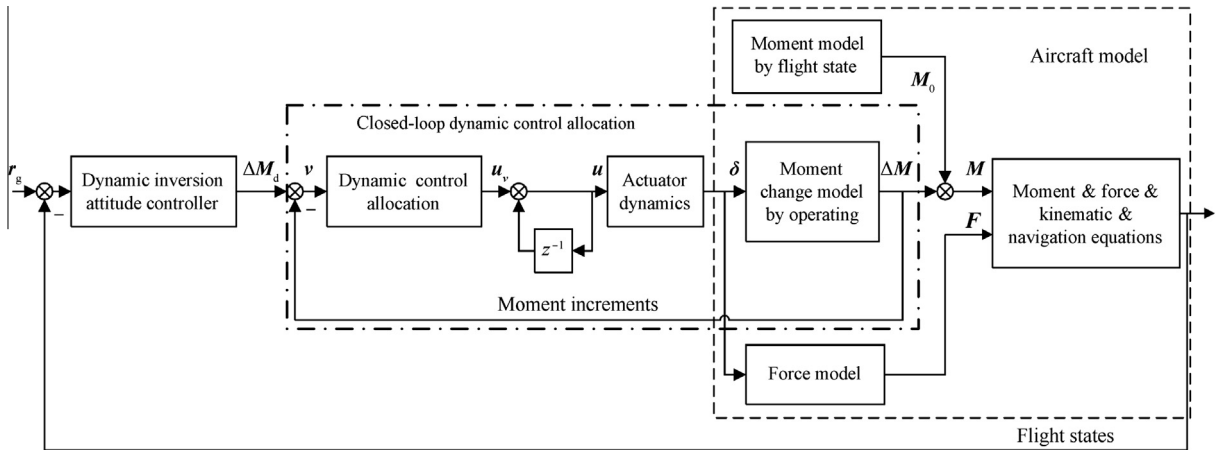


Fig. 1 Closed-loop dynamic control allocation configuration.

$$\begin{cases} c_1 = [(J_y - J_z)J_z - J_{xz}^2]/\Gamma \\ c_2 = (J_x - J_y + J_z)/\Gamma; \quad c_3 = J_z/\Gamma \\ c_4 = J_{xz}/\Gamma; \quad c_5 = (J_z - J_x)/J_y; \quad c_6 = J_{xz}/J_y \\ c_7 = 1/J_y; \quad c_8 = [J_x(J_x - J_y) + J_{xz}^2]/\Gamma \\ c_9 = J_x/\Gamma; \quad \Gamma = J_x J_z - J_{xz}^2 \end{cases} \quad (6)$$

where  $J_i$  ( $i = x, y, z$ ) is the moment of inertia about  $i$  axis, and  $J_{xz}$  the cross-product of inertia;  $M_x$ ,  $M_y$  and  $M_z$  are the roll, pitch, and yaw moments, which can be described as

$$\begin{cases} M_x = \rho V^2 S b C_l / 2 \\ M_y = \rho V^2 S \bar{c} C_m / 2 \\ M_z = \rho V^2 S b C_n / 2 \end{cases} \quad (7)$$

where  $\rho$  is the air density,  $V$  the flight velocity,  $S$  the wing reference area,  $b$  the wing span, and  $\bar{c}$  the wing mean geometric chord;  $C_l$ ,  $C_m$  and  $C_n$  are the roll, pitch and yaw moment coefficients.

In Eq. (3),  $F_x$ ,  $F_y$  and  $F_z$  are the components of the resultant force including aerodynamic force and engine thrust along the body axes, and they are defined by

$$\begin{cases} F_x = P + L \sin \alpha - Y \cos \alpha \sin \beta - D \cos \alpha \cos \beta \\ F_y = Y \cos \beta - D \sin \beta \\ F_z = -L \cos \alpha - Y \sin \alpha \sin \beta - D \sin \alpha \cos \beta \end{cases} \quad (8)$$

where  $\alpha$  and  $\beta$  are the angles of attack and sideslip; the engine thrust  $P = C_p \delta_p$ , where  $C_p$  is the thrust coefficient, and  $\delta_p$  the throttle setting;  $D$ ,  $L$  and  $Y$  are the drag, lift and side-force, which can be described as

$$\begin{cases} D = \rho V^2 S C_D / 2 \\ L = \rho V^2 S C_L / 2 \\ Y = \rho V^2 S C_Y / 2 \end{cases} \quad (9)$$

where  $C_D$ ,  $C_L$  and  $C_Y$  are the drag, lift and side-force coefficients.

The expressions of  $\mathbf{M}_0$  and  $\Delta \mathbf{M}$  in Fig. 1 will be given in the following text. According to Eq. (1), the roll, pitch, and yaw moments  $M_x$ ,  $M_y$  and  $M_z$  can be respectively separated into two parts as follows:

$$\begin{cases} M_x = M_x^0 + \Delta M_x \\ M_y = M_y^0 + \Delta M_y \\ M_z = M_z^0 + \Delta M_z \end{cases} \quad (10)$$

where  $\Delta M_x$ ,  $\Delta M_y$  and  $\Delta M_z$  are the moment increments produced by control surface deflections, and  $\mathbf{M}_0 = [M_x^0 \quad M_y^0 \quad M_z^0]^T$  is given by

$$\begin{cases} M_x^0 = \rho V^2 S b (C_{l\beta} \beta + C_{l\bar{p}} \bar{p} + C_{l\bar{r}} \bar{r}) / 2 \\ M_y^0 = \rho V^2 S \bar{c} (C_{m,\alpha=0} + C_{m\alpha} \alpha + C_{m\bar{q}} \bar{q} + C_{m\bar{\alpha}} \bar{\alpha}) / 2 \\ M_z^0 = \rho V^2 S b (C_{n\beta} \beta + C_{n\bar{p}} \bar{p} + C_{n\bar{r}} \bar{r}) / 2 \end{cases} \quad (11)$$

where  $C_{(*)}$  is the aerodynamic derivatives;  $\bar{p}$ ,  $\bar{q}$ ,  $\bar{r}$  and  $\bar{\alpha}$  are defined by

$$\begin{cases} \bar{p} = pb/(2V), \quad \bar{r} = rb/(2V) \\ \bar{q} = q\bar{c}/(2V), \quad \bar{\alpha} = \dot{\alpha}\bar{c}/(2V) \end{cases} \quad (12)$$

and  $\dot{\alpha}$  is the derivative of the angle of attack.

Substituting Eqs. (10)–(12) into Eq. (2), Eq. (2) can be rewritten in the affine nonlinear form

$$\begin{bmatrix} \dot{p} \\ \dot{q} \\ \dot{r} \end{bmatrix} = \begin{bmatrix} f_p \\ f_q \\ f_r \end{bmatrix} + \mathbf{B}_c \begin{bmatrix} \Delta M_x \\ \Delta M_y \\ \Delta M_z \end{bmatrix} \quad (13)$$

where  $f_p$ ,  $f_q$ ,  $f_r$  and  $\mathbf{B}_c$  are

$$\begin{cases} f_p = (c_1 r + c_2 p) q + c_3 M_x + c_4 M_z \\ f_q = c_5 p r - c_6 (p^2 - r^2) + c_7 M_y \\ f_r = (c_8 p - c_2 r) q + c_4 M_x + c_9 M_z \\ \mathbf{B}_c = \begin{bmatrix} c_3 & 0 & c_4 \\ 0 & c_7 & 0 \\ c_4 & 0 & c_9 \end{bmatrix} \end{cases} \quad (14)$$

We suppose  $\Delta \mathbf{M} = [\Delta M_x \quad \Delta M_y \quad \Delta M_z]^T$ , and according to Eq. (13), the actual moment increments  $\Delta \mathbf{M}$  is derived by

$$\Delta \mathbf{M} = \mathbf{B}_c^{-1} [\dot{p} - f_p \quad \dot{q} - f_q \quad \dot{r} - f_r]^T \quad (15)$$

where  $\dot{p}$ ,  $\dot{q}$  and  $\dot{r}$  are measured by the angular acceleration sensors.

## 2.2. Dynamic inversion attitude controller design

Having separated the attitude states into fast and slow dynamics, the feedback is used to provide the system with desirable dynamics. The fast dynamics of the aircraft attitude has been given in Eq. (2). And the desired attitude angular rates dynamics is specified by<sup>1</sup>

$$\begin{bmatrix} \dot{p}_d \\ \dot{q}_d \\ \dot{r}_d \end{bmatrix} = \begin{bmatrix} \omega_p & 0 & 0 \\ 0 & \omega_q & 0 \\ 0 & 0 & \omega_r \end{bmatrix} \begin{bmatrix} p_c - p \\ q_c - q \\ r_c - r \end{bmatrix} \quad (16)$$

where  $\omega_p$ ,  $\omega_q$  and  $\omega_r$  are the design parameters;  $p_c$ ,  $q_c$ , and  $r_c$  the commanded angular rates given by the slow dynamics loop.

Replacing the  $[\dot{p} \quad \dot{q} \quad \dot{r}]^T$  in the left of Eq. (13) by  $[\dot{p}_d \quad \dot{q}_d \quad \dot{r}_d]^T$  from Eq. (16), we can derive the desired moment increment  $\Delta \mathbf{M}_d$ :

$$\Delta \mathbf{M}_d = \mathbf{B}_c^{-1} [\dot{p}_d - f_p \quad \dot{q}_d - f_q \quad \dot{r}_d - f_r]^T \quad (17)$$

The slow dynamics of the aircraft attitude has been given in Eq. (4). And the desired attitude angular dynamics is similar to Eq. (16):

$$\begin{bmatrix} \dot{\phi}_d \\ \dot{\theta}_d \\ \dot{\psi}_d \end{bmatrix} = \begin{bmatrix} \omega_\phi & 0 & 0 \\ 0 & \omega_\theta & 0 \\ 0 & 0 & \omega_\psi \end{bmatrix} \begin{bmatrix} \phi_c - \phi \\ \theta_c - \theta \\ \psi_c - \psi \end{bmatrix} \quad (18)$$

where  $\omega_\phi$ ,  $\omega_\theta$  and  $\omega_\psi$  are the design parameters;  $\phi_c$ ,  $\theta_c$ , and  $\psi_c$  the commanded attitude angles given by designer.

Replacing  $[\dot{\phi} \quad \dot{\theta} \quad \dot{\psi}]^T$  in the left of Eq. (4) by  $[\dot{\phi}_d \quad \dot{\theta}_d \quad \dot{\psi}_d]^T$  from Eq. (18), we can derive the commanded angular rates  $[p_c \quad q_c \quad r_c]^T$  as follows:

$$\begin{bmatrix} p_c \\ q_c \\ r_c \end{bmatrix} = \begin{bmatrix} 1 & \tan \theta \sin \phi & \tan \theta \cos \phi \\ 0 & \cos \phi & -\sin \phi \\ 0 & \sin \phi / \cos \theta & \cos \phi / \cos \theta \end{bmatrix}^{-1} \begin{bmatrix} \dot{\phi}_d \\ \dot{\theta}_d \\ \dot{\psi}_d \end{bmatrix} \quad (19)$$

### 2.3. Control allocation problem

The objective of control allocation is to determine the actual control vector  $\mathbf{u} \in \mathbf{R}^m$  according to the virtual control vector  $\mathbf{v} \in \mathbf{R}^l$ , where  $m > l$ .

Mathematically, given  $\mathbf{v}(t)$ , then  $\mathbf{u}(t)$  is derived by

$$f(\mathbf{u}(t)) = \mathbf{v}(t) \quad (20)$$

where  $f: \mathbf{R}^m \mapsto \mathbf{R}^l$  is the nonlinear mapping from  $\mathbf{u}(t)$  to  $\mathbf{v}(t)$ . The actuator dynamics can be described as

$$\dot{\delta} = g(\delta, \mathbf{u}) \quad (21)$$

where  $\delta \in \mathbf{R}^m$  is the actuator deflection, and Eq. (21) is subject to a set of constraints

$$\delta_{\min} \leq \delta \leq \delta_{\max}, \quad |\dot{\delta}| \leq \dot{\delta}_{\max} \quad (22)$$

where  $\delta_{\min}$ ,  $\delta_{\max}$  and  $\dot{\delta}_{\max}$  are the lower and upper actuator position and rate constraints, respectively. Due to the typically fast actuator dynamics, we assume  $\delta = \mathbf{u}$ .

In a digital flight control system, it is reasonable to transform the actuator constraints from Eq. (22) to the following formula<sup>16</sup>:

$$\begin{cases} \underline{\mathbf{u}}(t) \leq \mathbf{u}(t) \leq \bar{\mathbf{u}}(t) \\ \underline{\mathbf{u}}(t) = \max(\delta_{\min}, (\mathbf{u}(t-T) - \dot{\delta}_{\max}T)) \\ \bar{\mathbf{u}}(t) = \min(\delta_{\max}, (\mathbf{u}(t-T) + \dot{\delta}_{\max}T)) \end{cases} \quad (23)$$

where  $T$  is the sample time.

### 2.4. Analytical solution of closed-loop dynamic control allocation

The dynamic control allocation can be expressed as the following sequential quadratic-programming problem if no actuators are saturated.

$$\begin{cases} \mathbf{u}_v(t) = \arg \min_{\mathbf{u}_v(t) \in \Omega} \{ \|\mathbf{W}_1(\mathbf{u}_v(t) - \mathbf{u}_s(t))\|^2 + \|\mathbf{W}_2(\mathbf{u}_v(t) - \mathbf{u}_v(t-T))\|^2 \} \\ \Omega = \arg \min_{\underline{\mathbf{u}}(t) \leq \mathbf{u}_v(t) \leq \bar{\mathbf{u}}(t)} \|\mathbf{W}_\Omega(\mathbf{B}\mathbf{u}_v(t) - \mathbf{v}(t))\| \end{cases} \quad (24)$$

where  $\mathbf{u}_s(t) \in \mathbf{R}^m$  is the desired steady-state control input;  $\mathbf{W}_1$ ,  $\mathbf{W}_2$  and  $\mathbf{W}_\Omega$  are the square matrices of proper dimensions;  $\|\mathbf{x}\|$  denotes the Euclidean norm defined by  $\|\mathbf{x}\| = \sqrt{\mathbf{x}^T \mathbf{x}}$ .

**Lemma 1.** (Ref.<sup>12</sup>) Let us remove the constraints of actuators, then the closed form solution to Eq. (24) is

$$\mathbf{u}_v(k) = \mathbf{E}\mathbf{u}_s(k) + \mathbf{F}\mathbf{u}_v(k-1) + \mathbf{G}\mathbf{v}(k) \quad (25)$$

where

$$\begin{cases} \mathbf{E} = (\mathbf{I} - \mathbf{G}\mathbf{B})\mathbf{W}^{-2}\mathbf{W}_1^2 \\ \mathbf{F} = (\mathbf{I} - \mathbf{G}\mathbf{B})\mathbf{W}^{-2}\mathbf{W}_2^2 \\ \mathbf{G} = \mathbf{W}^{-1}(\mathbf{B}\mathbf{W}^{-1})^\dagger \\ \mathbf{W} = \sqrt{\mathbf{W}_1^2 + \mathbf{W}_2^2} \end{cases} \quad (26)$$

where  $\mathbf{I}$  is the identity matrix, and the symbol “ $\dagger$ ” denotes the pseudoinverse operator defined as  $\mathbf{A}^\dagger = \mathbf{A}^T(\mathbf{A}\mathbf{A}^T)^{-1}$ .

In the steady-state, we assume the error  $\mathbf{v}(k) = \Delta\mathbf{M}_d(k) - \Delta\mathbf{M}(k)$  is zero, therefore, the desired control input  $\mathbf{u}_s(k) = \mathbf{0}$ , and  $\mathbf{u}_v(k) = \mathbf{u}_r(k-1)$ .

Then, Eq. (25) reduces to

$$\mathbf{u}_v(k) = (\mathbf{I} - \mathbf{F})^{-1}\mathbf{G}\mathbf{v}(k) \quad (27)$$

The input of actuator  $\mathbf{u}(k)$  in Fig. 1 is

$$\mathbf{u}(k) = \mathbf{u}(k-1) + \mathbf{u}_v(k) \quad (28)$$

## 3. Stability for closed-loop dynamic control allocation

The stability for the closed-loop dynamic control allocation system is of significant importance. In order to validate the stability, the input-output relation of closed-loop dynamic control allocation is given in the following text.

The actual moment increment  $\Delta\mathbf{M}(k)$  can be derived by

$$\Delta\mathbf{M}(k) = \mathbf{B}_r(k)\mathbf{u}(k) \quad (29)$$

where  $\mathbf{B}_r(k)$  is the actual control effectiveness matrix, which is changed with different flight conditions.

Substituting Eqs. (27) and (28) into Eq. (29), we have

$$\Delta\mathbf{M}(k) = \mathbf{B}_r(k)\mathbf{u}(k-1) + \mathbf{B}_r(k)(\mathbf{I} - \mathbf{F})^{-1}\mathbf{G}\mathbf{v}(k) \quad (30)$$

where the input of dynamic control allocation  $\mathbf{v}(k)$  is given by  $\mathbf{v}(k) = \Delta\mathbf{M}_d(k) - \Delta\mathbf{M}(k)$

The change of  $\mathbf{B}_r(k)$  is small during the sample time, we obtain

$$\mathbf{B}_r(k) = \mathbf{B}_r(k-1) \quad (32)$$

Then substituting Eqs. (29), (31) and (32) into Eq. (30), we have

$$\Delta\mathbf{M}(k) = \Delta\mathbf{M}(k-1) + \mathbf{V}(k)(\Delta\mathbf{M}_d(k) - \Delta\mathbf{M}(k)) \quad (33)$$

where

$$\mathbf{V}(k) = \mathbf{B}_r(k)(\mathbf{I} - \mathbf{F})^{-1}\mathbf{G}, \quad \mathbf{V} \in \mathbf{R}^{l \times l} \quad (34)$$

The input-output relation of closed-loop dynamic control allocation is obtained according to the  $z$  transform of Eq. (33):

$$\frac{\Delta\mathbf{M}(z)}{\Delta\mathbf{M}_d(z)} = \frac{z\mathbf{V}(z)}{z(\mathbf{I} + \mathbf{V}(z)) - \mathbf{I}} \quad (35)$$

### 3.1. Stability in the absence of actuator failures

In this part, we consider the stability for closed-loop dynamic control allocation when the actuators are healthy.

**Lemma 2** (Schur Lemma). Given  $\mathbf{A} \in \mathbf{R}^{n \times n}$  with eigenvalues  $\lambda_1, \lambda_2, \dots, \lambda_n$  in any prescribed order, there is an orthogonal matrix  $\mathbf{P} \in \mathbf{E}^{n \times n}$ , where  $\mathbf{E}$  is the set of orthogonal matrix. And we have

$$\mathbf{P}^{-1}\mathbf{A}\mathbf{P} = \mathbf{B} = \begin{bmatrix} b_{11} & b_{12} & \cdots & b_{1n} \\ 0 & b_{22} & \cdots & b_{2n} \\ \vdots & \ddots & \ddots & \vdots \\ 0 & \cdots & 0 & b_{nn} \end{bmatrix}$$

is upper triangular, with diagonal entries  $b_{ii} = \lambda_i$  ( $i = 1, 2, \dots, n$ ).

**Theorem 1.** Let the closed form solution to Eq. (24) be defined in Lemma 1, and the closed-loop dynamic control allocation system is described as Eq. (35). And  $\lambda_i$  ( $i = 1, 2, \dots, n$ ) is the eigenvalue of  $V(z)$ . The closed-loop dynamic control allocation is stable if  $|1 + \lambda_i| > 1$  is satisfied.

**Proof.** According to Eq. (35), the stability of the closed-loop allocation system is determined by the locations of the closed-loop poles or the roots of characteristic equation in the  $z$  plane. The characteristic equation is

$$z(\mathbf{I} + \mathbf{V}(z)) - \mathbf{I} = \mathbf{0} \quad (36)$$

And the system is stable if any of the closed-loop characteristic roots lie inside the unit circle.

Considering Lemma 2, we obtain

$$\mathbf{V}(z) = \mathbf{P} \begin{bmatrix} \lambda_1 & b_{12} & \cdots & \cdots & b_{1n} \\ \mathbf{0} & \lambda_2 & b_{22} & \cdots & b_{2n} \\ \vdots & & \ddots & \ddots & \vdots \\ \vdots & & & \ddots & b_{n-1,n} \\ \mathbf{0} & 0 & \cdots & 0 & \lambda_n \end{bmatrix} \mathbf{P}^{-1} \quad (37)$$

Substituting Eq. (37) into Eq. (36), we have

$$\begin{aligned} & z\mathbf{P}\mathbf{P}^{-1} + z\mathbf{P} \begin{bmatrix} \lambda_1 & b_{12} & \cdots & \cdots & b_{1n} \\ 0 & \lambda_2 & b_{22} & \cdots & b_{2n} \\ \vdots & & \ddots & \ddots & \vdots \\ \vdots & & & \ddots & b_{n-1,n} \\ 0 & 0 & \cdots & 0 & \lambda_n \end{bmatrix} \mathbf{P}^{-1} - \mathbf{P}\mathbf{P}^{-1} \\ & = \mathbf{P} \left( z\mathbf{I} + z \begin{bmatrix} \lambda_1 & b_{12} & \cdots & \cdots & b_{1n} \\ 0 & \lambda_2 & b_{22} & \cdots & b_{2n} \\ \vdots & & \ddots & \ddots & \vdots \\ \vdots & & & \ddots & b_{n-1,n} \\ 0 & 0 & \cdots & 0 & \lambda_n \end{bmatrix} - \mathbf{I} \right) \mathbf{P}^{-1} = \mathbf{0} \end{aligned} \quad (38)$$

The characteristic equation becomes

$$z_i + z_i\lambda_i - 1 = 0 \quad (i = 1, 2, \dots, n) \quad (39)$$

The roots of characteristic equation are found to be

$$z_i = \frac{1}{1 + \lambda_i} \quad (i = 1, 2, \dots, n) \quad (40)$$

If  $|z_i| < 1$ , then the system is stable and we obtain

$$|1 + \lambda_i| > 1 \quad (41)$$

This completes the proof.  $\square$

### 3.2. Stability in the presence of actuator failures

The stability condition for closed-loop control allocation is given in Theorem 1 when the actuators are healthy. However, the actuators of an aircraft can be affected by many types of failures in the flight missions. And there are two typical failures

which are the loss of effectiveness and lock-in-place failures. Both of them are considered here.

**Assumption 1.** Two actuator failures do not happen simultaneously.

The control signal  $\delta(t)$  (input to the plant, output of the actuator) can be described as the following formula to incorporate the actuator failures.

$$\begin{cases} \delta(t) = (\mathbf{\Xi} + \mathbf{\Phi}_u)\mathbf{u}(t) + \mathbf{\Phi}_w\mathbf{w}(t) \\ \mathbf{\Xi} = \text{diag}(d_1^e, d_2^e, \dots, d_m^e), \quad 0 < d_i^e \leq 1 \\ \mathbf{\Phi}_u = \text{diag}(d_1^u, d_2^u, \dots, d_m^u), \quad d_i^u = \{0, 1\} \\ \mathbf{\Phi}_w = \text{diag}(d_1^w, d_2^w, \dots, d_m^w), \quad d_i^w = \{0, 1\} \\ \mathbf{w} = [w_1 \ w_2 \ \cdots \ w_m]^T, \quad \delta_{\min}^i \leq w_i \leq \delta_{\max}^i \end{cases} \quad (42)$$

where  $\delta_{\min}^i$  and  $\delta_{\max}^i$  present the  $i$ th element of  $\delta_{\min}$  and  $\delta_{\max}$  in Eq. (22), respectively. And the actuator  $i$  has a loss of effectiveness failure if  $0 < d_i^e < 1$ ,  $d_j^e = 1$ ,  $j \neq i$  and  $\mathbf{\Phi}_u = \mathbf{\Phi}_w = \mathbf{0}$ ; the actuator  $i$  is stuck at the degree  $w_i$  if  $d_i^u = 0$ ,  $d_j^u = 1$ ,  $d_i^w = 1$ ,  $d_j^w = 0$ ,  $j \neq i$  and  $\mathbf{\Xi} = \mathbf{0}$ .

In the presence of the actuator loss of effectiveness failure, the actual moment increment  $\Delta\mathbf{M}(k)$  will be changed. Considering Eqs. (29) and (42), we have

$$\Delta\mathbf{M}(k) = \mathbf{B}_r(k)\mathbf{\Xi}\mathbf{u}(k) = \mathbf{B}_r(k)\mathbf{u}(k) \quad (43)$$

We can see from Eq. (43) the actuator failures change the control effectiveness matrix. And the changed control effectiveness matrix  $\mathbf{B}_r$  can be written as

$$\mathbf{B}_r(k) = \mathbf{B}_r^0(k) + \Delta\mathbf{B}_r(k) \quad (44)$$

where  $\mathbf{B}_r^0(k)$  is the control effectiveness matrix without failures, and  $\Delta\mathbf{B}_r(k)$  the control effectiveness matrix change produced by the actuator loss of effectiveness failure. Substituting Eq. (44) into Eq. (34), we have

$$\mathbf{V}(k) = (\mathbf{B}_r^0(k) + \Delta\mathbf{B}_r(k))(\mathbf{I} - \mathbf{F})^{-1}\mathbf{G} = \mathbf{V}_0(k) + \Delta\mathbf{V}(k) \quad (45)$$

where  $\mathbf{V}_0(k) = \mathbf{B}_r^0(k)(\mathbf{I} - \mathbf{F})^{-1}\mathbf{G}$  is the matrix without failures, and the error caused by the actuator loss of effectiveness failure is

$$\Delta\mathbf{V}(k) = \Delta\mathbf{B}_r(k)(\mathbf{I} - \mathbf{F})^{-1}\mathbf{G} \quad (46)$$

**Assumption 2.** The  $\mathbf{V}_0(k)$  and  $\Delta\mathbf{V}(k)$  commute, and have eigenvalues  $\lambda_1^0, \lambda_2^0, \dots, \lambda_n^0$  and  $\lambda_1^\Delta, \lambda_2^\Delta, \dots, \lambda_n^\Delta$ , respectively.

**Corollary 1.** The actuator loss of effectiveness failure happens. Considering Eqs. (35), (45) and Assumption 2, if the eigenvalues  $\lambda_i^\Delta$  ( $i = 1, 2, \dots, n$ ) of the error matrix  $\Delta\mathbf{V}(k)$  and the eigenvalues  $\lambda_i^0$  ( $i = 1, 2, \dots, n$ ) of the matrix  $\mathbf{V}_0(k)$  satisfy the following formula:

$$\lambda_i^\Delta > -\lambda_i^0 \quad \text{or} \quad \lambda_i^\Delta < -(\lambda_i^0 + 2) \quad (47)$$

then the closed-loop dynamic control allocation is stable in the presence of the actuator loss of effectiveness failure.

**Proof.** According to Assumption 2, the eigenvalues of  $\mathbf{V}_0(k) + \Delta\mathbf{V}(k)$  are  $\lambda_i^0 + \lambda_i^\Delta$  ( $i = 1, 2, \dots, n$ ).

The actual control effectiveness matrix changes in the presence of the actuator loss of effectiveness failure; however, the stability of the closed-loop system is desired.

Considering Theorem 1, we obtain

$$|\lambda_i^A + \lambda_i^0 + 1| > 1 \Rightarrow \lambda_i^A > -\lambda_i^0 \quad \text{or} \quad \lambda_i^A < -(\lambda_i^0 + 2) \quad (48)$$

This completes the proof.  $\square$

In the presence of the actuator lock-in-place failure, the actuator  $i$  is stuck at the degree  $w_i$ . It is equivalent to adding the disturbance to the actual moment increment  $\Delta \mathbf{M}(k)$ . Considering Eqs. (29) and (42), we have

$$\Delta \mathbf{M}(k) = \mathbf{B}_r(k)(\Phi_u \mathbf{u}(k) + \Phi_w \mathbf{w}(k)) \quad (49)$$

**Corollary 2.** *The actuator lock-in-place failure happens. If the eigenvalues  $\lambda_i^u$  of the matrix  $\mathbf{V}_u(k)$  satisfy the following formula:*

$$|1 + \lambda_i^u| > 1 \quad (i = 1, 2, \dots, n) \quad (50)$$

where

$$\mathbf{V}_u(k) = \mathbf{B}_r(k)\Phi_u(\mathbf{I} - \mathbf{F})^{-1}\mathbf{G} \quad (51)$$

and the steady-state inputs of actuator  $\mathbf{u}(\infty)$  satisfy

$$\begin{aligned} \mathbf{B}_r(\infty)(\Phi_u \mathbf{u}(\infty) + \Phi_w \mathbf{w}(\infty)) &= \mathbf{0} \\ (\delta_{\min} \leq \mathbf{u}(\infty), \mathbf{w}(\infty) \leq \delta_{\max}) \end{aligned} \quad (52)$$

then the closed-loop dynamic control allocation is stable in the presence of the actuator lock-in-place failure.

**Proof.** Substituting Eqs. (27) and (28) into Eq. (49), we have

$$\begin{aligned} \Delta \mathbf{M}(k) &= \mathbf{B}_r(k)[\Phi_u(\mathbf{u}(k-1) + (\mathbf{I} - \mathbf{F})^{-1}\mathbf{G}\mathbf{v}(k)) \\ &\quad + \Phi_w \mathbf{w}(k)] \end{aligned} \quad (53)$$

We derive  $\mathbf{w}(k) = \mathbf{w}(k-1)$  because the actuator is stuck. And according to Eqs. (32), (33), and (53), we have

$$\Delta \mathbf{M}(k) = \Delta \mathbf{M}(k-1) + \mathbf{V}_u(k)(\Delta \mathbf{M}_d(k) - \Delta \mathbf{M}(k)) \quad (54)$$

where the matrix  $\mathbf{V}_u(k)$  is given in Eq. (51).

Considering Theorem 1, we obtain  $|1 + \lambda_i^u| > 1$ .

Otherwise, the steady-state moment increment  $\Delta \mathbf{M}(\infty) = \mathbf{0}$ . According to Eq. (49), we have

$$\mathbf{B}_r(\infty)(\Phi_u \mathbf{u}(\infty) + \Phi_w \mathbf{w}(\infty)) = \mathbf{0} \quad (55)$$

and  $\mathbf{u}(\infty)$  and  $\mathbf{w}(\infty)$  must satisfy the following position limits of the actuators:

$$\delta_{\min} \leq \mathbf{u}(\infty), \mathbf{w}(\infty) \leq \delta_{\max} \quad (56)$$

which completes the proof.  $\square$

#### 4. Simulation results

In this section, we consider a canard rotor/wing (CRW) aircraft model (see Refs. <sup>17,18</sup> for more details) in the fixed-wing mode. The simulation model includes the moment, force, kinematic and navigation equations in Eqs. (2)–(5). And the specific aerodynamic force and moment coefficients of the CRW in the fixed-wing mode are given by

$$\begin{cases} C_L = C_{L0} + C_{L\alpha}\alpha + C_{L\delta_c}\delta_c + C_{L\delta_e}\delta_e \\ C_D = C_{D1}C_L^2 + C_{D2}C_L + C_{D3} \\ C_Y = C_{Y\beta}\beta + C_{Y\delta_{rL}}\delta_{rL} + C_{Y\delta_{rR}}\delta_{rR} \end{cases} \quad (57)$$

$$\begin{cases} C_l = C_{l\delta_{aL}}\delta_{aL} + C_{l\delta_{aR}}\delta_{aR} + C_{l\delta_{rL}}\delta_{rL} + C_{l\delta_{rR}}\delta_{rR} \\ \quad + C_{l\beta}\beta + C_{l\bar{p}}\bar{p} + C_{l\bar{r}}\bar{r} \\ C_m = C_{m1}C_L^2 + C_{m2}C_L + C_{m3} + C_{m\delta_c}\delta_c + C_{m\delta_e}\delta_e \\ \quad + C_{m\bar{q}}\bar{q} + C_{m\bar{z}}\bar{z} \\ C_n = C_{n\delta_{aL}}\delta_{aL} + C_{n\delta_{aR}}\delta_{aR} + C_{n\delta_{rL}}\delta_{rL} + C_{n\delta_{rR}}\delta_{rR} \\ \quad + C_{n\beta}\beta + C_{n\bar{p}}\bar{p} + C_{n\bar{r}}\bar{r} \end{cases} \quad (58)$$

where  $\alpha, \beta$  and  $\dot{\alpha}$  can be derived by

$$\begin{cases} \alpha = \arctan(V_z/V_x) \\ \beta = \arcsin(V_y/V) \\ \dot{\alpha} = [(V_x\dot{V}_z - V_z\dot{V}_x) \cos \alpha] / V_x^2 \end{cases} \quad (59)$$

where the flight velocity  $V = \sqrt{V_x^2 + V_y^2 + V_z^2}$ . In addition, we can derive  $\dot{\alpha}$  according to Eqs. (12) and (59). In addition, the thrust coefficient of this aircraft in the fixed-wing mode is  $C_P = 2487$ .

The aerodynamic parameters are shown in Table 1, while the wing-planform and inertia parameters are shown in Table 2. These parameters are derived from both Ref. <sup>19</sup> and aerodynamic computing in terms of the aircraft geometry figuration.

The control inputs consist of the deflections for the left aileron  $\delta_{aL}$ , the right aileron  $\delta_{aR}$ , the left rudder  $\delta_{rL}$  and the right rudder  $\delta_{rR}$  in the lateral direction. And the canard  $\delta_c$  and ele-

**Table 1** Aerodynamic parameters for the model.

| Parameter          | Value                  | Parameter          | Value                  |
|--------------------|------------------------|--------------------|------------------------|
| $C_{L0}$           | 0.224                  | $C_{Lz}$           | 0.115                  |
| $C_{L\delta_c}$    | 0.0610                 | $C_{L\delta_e}$    | 0.0196                 |
| $C_{D1}$           | 0.0815                 | $C_{D2}$           | -0.0465                |
| $C_{D3}$           | 0.0756                 | $C_{Y\beta}$       | $-9.60 \times 10^{-3}$ |
| $C_{Y\delta_{rL}}$ | $-1.45 \times 10^{-3}$ | $C_{Y\delta_{rR}}$ | $-1.45 \times 10^{-3}$ |
| $C_{l\delta_{aL}}$ | $2.50 \times 10^{-4}$  | $C_{l\delta_{aR}}$ | $-2.50 \times 10^{-4}$ |
| $C_{l\delta_{rL}}$ | 0                      | $C_{l\delta_{rR}}$ | 0                      |
| $C_{l\beta}$       | $-1.53 \times 10^{-3}$ | $C_{l\bar{p}}$     | -0.343                 |
| $C_{l\bar{r}}$     | $-5.54 \times 10^{-3}$ | $C_{m1}$           | -0.166                 |
| $C_{m2}$           | 0.147                  | $C_{m3}$           | -0.182                 |
| $C_{m\delta_c}$    | 0.0790                 | $C_{m\delta_e}$    | -0.0356                |
| $C_{m\bar{q}}$     | -57.1                  | $C_{m\bar{z}}$     | -11.6                  |
| $C_{n\delta_{aL}}$ | $9.00 \times 10^{-6}$  | $C_{n\delta_{aR}}$ | $-9.00 \times 10^{-6}$ |
| $C_{n\delta_{rL}}$ | $-9.65 \times 10^{-4}$ | $C_{n\delta_{rR}}$ | $-9.65 \times 10^{-4}$ |
| $C_{n\beta}$       | $-2.4 \times 10^{-3}$  | $C_{n\bar{p}}$     | $8.46 \times 10^{-3}$  |
| $C_{n\bar{r}}$     | -0.560                 |                    |                        |

**Table 2** Wing-planform and inertia parameters for the model.

| Parameter                  | Value | Parameter                     | Value |
|----------------------------|-------|-------------------------------|-------|
| $b$ (m)                    | 2.80  | $S$ (m <sup>2</sup> )         | 1.21  |
| $\bar{c}$ (m)              | 0.40  | $m$ (kg)                      | 450   |
| $J_x$ (kg·m <sup>2</sup> ) | 72.5  | $J_y$ (kg·m <sup>2</sup> )    | 246.6 |
| $J_z$ (kg·m <sup>2</sup> ) | 140.5 | $J_{xz}$ (kg·m <sup>2</sup> ) | 0     |

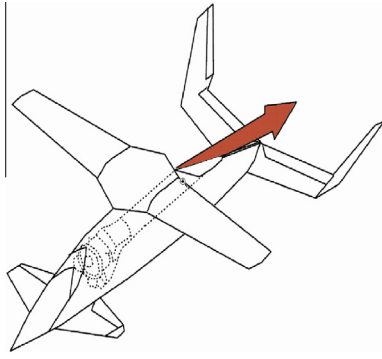


Fig. 2 CRW aircraft in the fixed wing mode.

vator  $\delta_e$  with different frequency characteristics are available for pitch control in the longitudinal direction. Fig. 2 shows the configuration of the CRW aircraft.<sup>20</sup>

The actuator dynamic is simplified to produce a simple first-order lag filter. The aileron, rudder, canard and elevator dynamics used in the simulation are described as

$$\begin{cases} \delta_{aL} = \frac{10}{s+10} u_{aL}, & \delta_{rL} = \frac{10}{s+10} u_{rL} \\ \delta_{aR} = \frac{10}{s+10} u_{aR}, & \delta_{rR} = \frac{10}{s+10} u_{rR} \\ \delta_c = \frac{20}{s+20} u_c, & \delta_e = \frac{10}{s+10} u_e \\ |\delta_{aL(R)}| \leq 25^\circ, & |\delta_{rL(R)}| \leq 25^\circ, \quad |\delta_c| \leq 15^\circ, \quad |\delta_e| \leq 25^\circ \end{cases} \quad (60)$$

where  $s$  denotes differential operator,  $\delta_{aL(R)}$  denotes  $\delta_{aL}$  or  $\delta_{aR}$ ,  $\delta_{rL(R)}$  is similar to  $\delta_{aL(R)}$ ,  $(u_{aL}, u_{aR}, u_{rL}, u_{rR}, u_c, u_e)$  and  $(\delta_{aL}, \delta_{aR}, \delta_{rL}, \delta_{rR}, \delta_c, \delta_e)$  are the input and output of the actuators, respectively. The canard actuator is faster than the elevator, whereas it is beneficial not to deflecting the canard at all to achieve low drag at trimmed flight. Thus, the canard is used to achieve the fast initial aircraft response, while the elevator is used solely at the trimmed flight. And we select the following constant matrix:

$$\begin{cases} \mathbf{W}_1 = \text{diag}(0.5, 0.5, 0.1, 0.1, 60, 37) \\ \mathbf{W}_2 = \text{diag}(0.4, 0.4, 0.8, 0.8, 0, 100) \end{cases} \quad (61)$$

The actual control effectiveness matrix without failures is given by

$$\mathbf{B}_f = 10^{-4} \begin{bmatrix} 2.50 & -2.50 & 0 & 0 & 0 & 0 \\ 0.09 & -0.09 & -9.65 & -9.65 & 0 & 0 \\ 0 & 0 & 0 & 0 & 790 & -356 \end{bmatrix} \quad (62)$$

The design matrix is  $\mathbf{B} = \mathbf{B}_f$ , whether the actuators are healthy or fail. However, the actual control effectiveness matrix  $\mathbf{B}_f$  changes when the actuator failures happen. The attitude controller parameters are  $\omega_\phi = 1.2$ ,  $\omega_\theta = 5$ ,  $\omega_\psi = 1.2$ ,  $\omega_p = 4.5$ ,  $\omega_q = 10$ ,  $\omega_r = 4.5$ , and the sample time is  $T = 0.02$  s.

In the following simulations, the initial altitude and velocity are 3000 m and 110 m/s, and the initial attitude angles and angular rates including  $\alpha$ ,  $\beta$ ,  $\phi$ ,  $\theta$ ,  $\psi$ ,  $p$ ,  $q$  and  $r$  are zeros. In addition, the throttle setting  $\delta_p = 0.2$ , while all the initial actuator deflections are zero.

#### 4.1. No actuator failures

Considering Eqs. (26), (34), (61) and (62), the eigenvalues of the matrix  $\mathbf{V}(k)$  are  $\lambda_1 = \lambda_2 = \lambda_3 = 1$ . According to Theorem 1, the designed closed-loop dynamic control allocation is stable. Figs. 3 and 4 show the attitude responses and actuator deflections using dynamic control allocation and closed-loop dynamic control allocation.

The two methods have the similar attitude tracking performance and actuator responses when there are no actuator failures. And the canard deflections are zero in steady state for

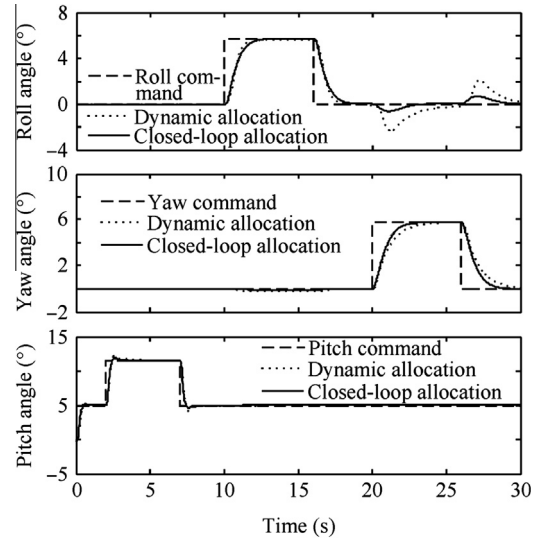


Fig. 3 Responses of attitude without failure.

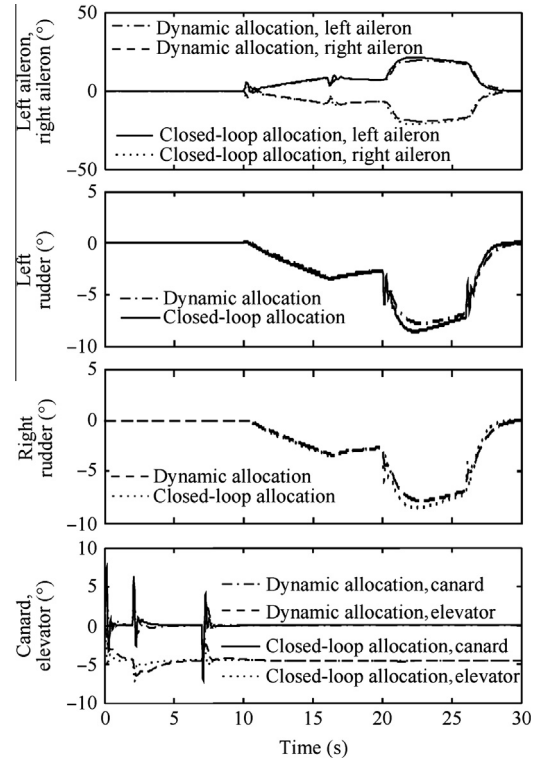


Fig. 4 Actuator deflections without failure.

two methods in Fig. 4. However, there is shorter rise time in the yaw response, and there is smaller effect on the roll response when the yaw angle changes using the closed-loop dynamic control allocation method in Fig. 3. And there are smaller overshoot and shorter settling time in the pitch response for the closed-loop dynamic control allocation.

#### 4.2. Actuator failures

Two failure cases are considered; however, there is no fault detection subsystem to identify the actuator failures in this research. We suppose the longitudinal- and lateral-directional equations are decoupled, and there is only one actuator which has only one type failure in one simulation. Therefore, the simulations of the different types of actuator failures in longitudinal direction and those in lateral direction are performed respectively.

The actual control effectiveness matrices,  $\mathbf{B}_{r\_lon} \in \mathbf{R}^{1 \times 2}$  and  $\mathbf{B}_{r\_lat} \in \mathbf{R}^{2 \times 4}$ , change while the design matrix,  $\mathbf{B}_{lon} \in \mathbf{R}^{1 \times 2}$  and  $\mathbf{B}_{lat} \in \mathbf{R}^{2 \times 4}$ , maintain constant after the actuator failure happens. And the weighting  $\mathbf{W}_{i\_lat} \in \mathbf{R}^{4 \times 4}$ ,  $\mathbf{W}_{i\_lon} \in \mathbf{R}^{2 \times 2}$  ( $i = 1, 2$ ) and design matrix are derived by Eqs. (61) and (62) using block matrix method.

$$\begin{cases} \mathbf{W}_1 = \text{diag}(\mathbf{W}_{1\_lat}, \mathbf{W}_{1\_lon}) \\ \mathbf{W}_2 = \text{diag}(\mathbf{W}_{2\_lat}, \mathbf{W}_{2\_lon}) \\ \mathbf{B}_r = \begin{bmatrix} \mathbf{B}_{lat} & \mathbf{0}_{2 \times 2} \\ \mathbf{0}_{1 \times 2} & \mathbf{B}_{lon} \end{bmatrix} \end{cases} \quad (63)$$

##### 4.2.1. Failure Case I: the loss of effectiveness failure

###### (1) Longitudinal actuator failure

The actuator failure is the loss of effectiveness failure of the elevator deflection in the pitch channel, while the canard is healthy. The elevator maintains only 50% of its effectiveness after 4 s, and we have the following formula according to Eq. (42).

$$\begin{bmatrix} \delta_c \\ \delta_e \end{bmatrix} = \begin{bmatrix} 1 & 0 \\ 0 & 0.5 \end{bmatrix} \begin{bmatrix} u_c \\ u_e \end{bmatrix} \quad (t \geq 4 \text{ s}) \quad (64)$$

Both longitudinal attitude tracking and actuator deflections are shown in Figs. 5 and 6.

Figs. 5 and 6 show that the dynamic control allocation method does not exactly distribute the desired pitch moment between canard and elevator after the failure happens. However, the closed-loop dynamic control allocation maintains

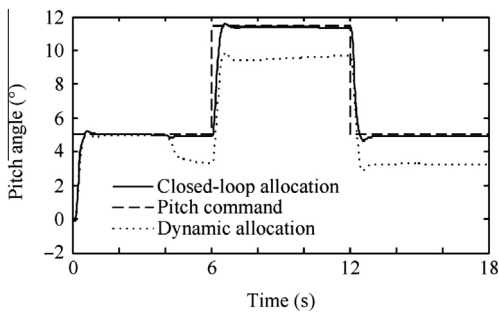


Fig. 5 Responses of pitch with elevator effectiveness loss.

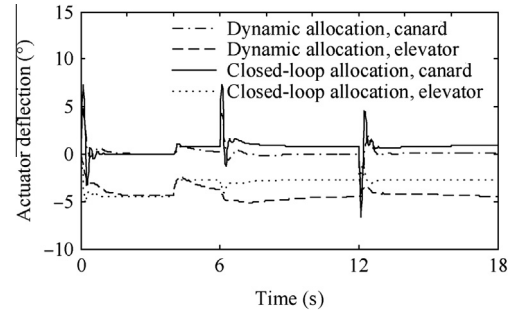


Fig. 6 Deflections of longitudinal actuators with elevator effectiveness loss.

the attitude tracking with little degradation, because there is a feedback from moment increment in the proposed approach, and the error between the desired and actual moment can be enforced to zero. To eliminate this error, the canard is used to compensate the elevator effectiveness loss. And the eigenvalues of  $\mathbf{V}_0(k)$  and  $\Delta \mathbf{V}(k)$  are  $\lambda_1^0 = 1$  and  $\lambda_1^\Delta = -0.17$ . According to Corollary 1, the closed-loop dynamic control allocation system is stable.

###### (2) Lateral actuator failure

The actuator failure is the loss of effectiveness failure of the right rudder deflection in the yaw channel, while the left rudder and ailerons are healthy. The right rudder maintains only 50% of its effectiveness after 12 s, and we have the following formula according to Eq. (42):

$$\begin{bmatrix} \delta_{aL} \\ \delta_{aR} \\ \delta_{rL} \\ \delta_{rR} \end{bmatrix} = \begin{bmatrix} 1 & & & \\ & 1 & & \\ & & 1 & \\ & & & 0.5 \end{bmatrix} \begin{bmatrix} u_{aL} \\ u_{aR} \\ u_{rL} \\ u_{rR} \end{bmatrix} \quad (t \geq 12 \text{ s}) \quad (65)$$

Both lateral attitude tracking and actuator deflections are shown in Figs. 7 and 8.

Fig. 7 shows that the desired lateral attitude commands, especially the yaw command, can be tracked by the proposed method after the failure happens. In Fig. 8, the deflections of all lateral actuators increase to derive the desired roll and yaw moments when the right rudder loses its effectiveness

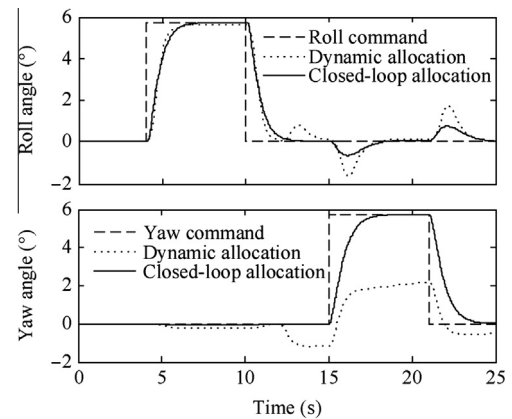
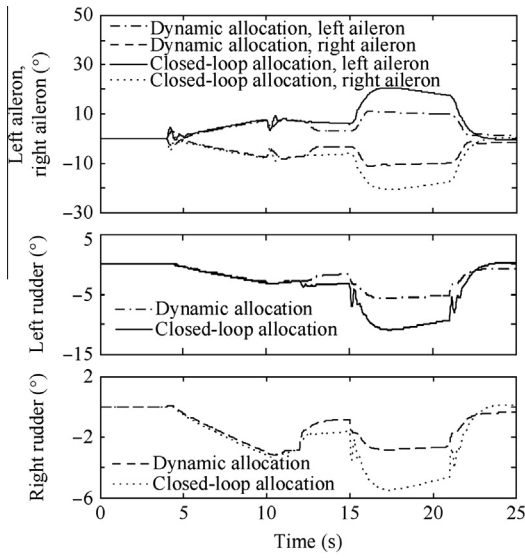


Fig. 7 Responses of lateral attitude with right rudder effectiveness loss.



**Fig. 8** Deflections of lateral actuators with right rudder effectiveness loss.

using the proposed method. And the eigenvalues of  $V_0(k)$  and  $\Delta V(k)$  are  $\lambda_1^0 = 1$ ,  $\lambda_1^\Delta = -0.25$ ,  $\lambda_2^0 = 1$  and  $\lambda_2^\Delta = 0$ . According to Corollary 1, the closed-loop dynamic control allocation system is stable.

#### 4.2.2. Failure Case II: lock-in-place failure

##### (1) Longitudinal actuator failure

The actuator failure is the lock-in-place failure of the elevator in the pitch channel, while the canard is healthy. The elevator is stuck at  $-3^\circ$  after 4 s, and we have the following formula according to Eq. (42).

$$\begin{bmatrix} \delta_c \\ \delta_e \end{bmatrix} = \begin{bmatrix} 1 & 0 \\ 0 & 0 \end{bmatrix} \begin{bmatrix} u_c \\ u_e \end{bmatrix} + \begin{bmatrix} 0 & 0 \\ 0 & 1 \end{bmatrix} \begin{bmatrix} 0 \\ -3 \end{bmatrix} \quad (t \geq 4 \text{ s}) \quad (66)$$

Both longitudinal attitude tracking and actuator deflections are shown in Figs. 9 and 10.

Fig. 9 shows that the dynamic control allocation method does not track the pitch command after the elevator is stuck at  $-3^\circ$ , and the attitude control system is unstable gradually. However, the proposed closed-loop dynamic control allocation maintains stability and attitude tracking after the failure hap-

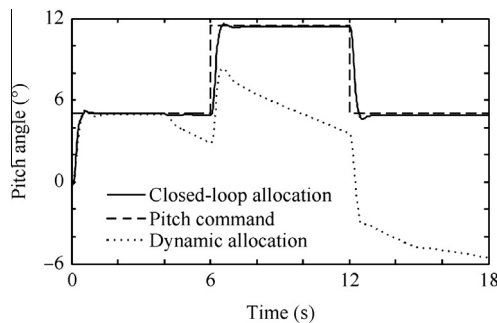


**Fig. 9** Responses of pitch with elevator stuck.

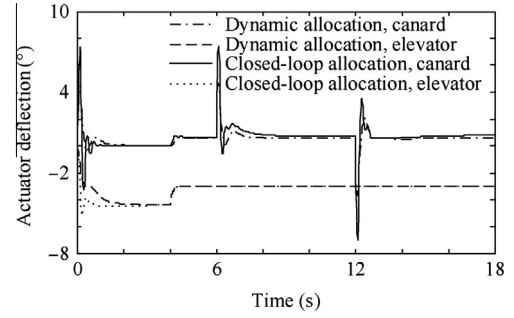


**Fig. 10** Deflections of longitudinal actuators with elevator stuck.

pens. We can see the canard in the two methods deflects to counteract the disturbance from the locked elevator in Fig. 10. However, the magnitude of canard deflection is larger and the response is faster in the proposed method. And the existence of feedback loop forces the moment increments error to zero. The eigenvalue of  $V_u(k)$  is 0.65, and  $\mathbf{u}(\infty) = [1.35^\circ - 3^\circ]^\top$ . According to Corollary 2, the closed-loop dynamic control allocation system is stable.

##### (2) Lateral actuator failure

The actuator failure is the lock-in-place failure of the left aileron in the roll channel, while the right aileron and rudders are healthy. The left aileron is stuck at  $10^\circ$  after 12 s, and we have the following equation according to Eq. (42):

$$\begin{bmatrix} \delta_{aL} \\ \delta_{aR} \\ \delta_{rL} \\ \delta_{rR} \end{bmatrix} = \begin{bmatrix} 0 & & & \\ & 1 & & \\ & & 1 & \\ & & & 1 \end{bmatrix} \begin{bmatrix} u_{aL} \\ u_{aR} \\ u_{rL} \\ u_{rR} \end{bmatrix} + \begin{bmatrix} 1 & & & \\ & 0 & & \\ & & 0 & \\ & & & 0 \end{bmatrix} \begin{bmatrix} 10 \\ 0 \\ 0 \\ 0 \end{bmatrix} \quad (t \geq 12 \text{ s}) \quad (67)$$

Both lateral attitude tracking and actuator deflections are shown in Figs. 11 and 12.

Fig. 11 shows that the desired lateral attitude commands, especially the roll command, cannot be tracked by the dynamic control allocation method after the failure happens. In Fig. 12, we can see the right aileron deflects to counteract the disturbance from the locked left aileron and derive the desired roll moment using the proposed method. Meanwhile, the left and right rudders deflect to derive the desired yaw moment and

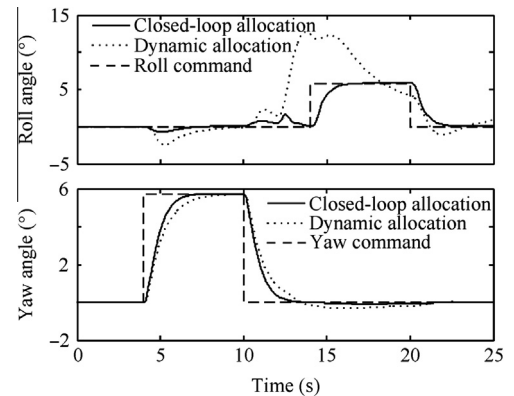


**Fig. 11** Responses of lateral attitude with left aileron stuck.

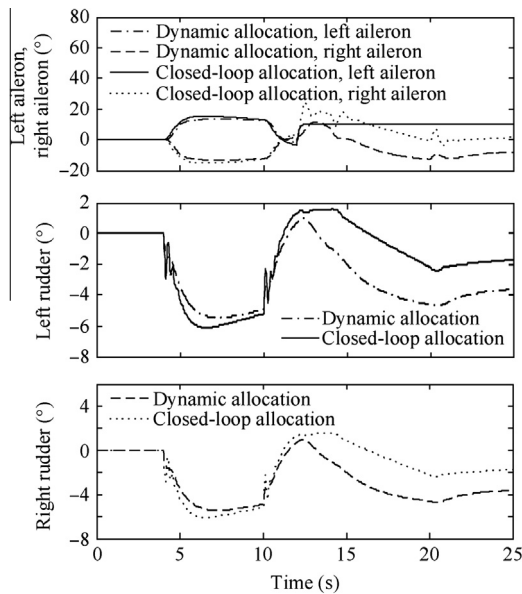


Fig. 12 Deflections of lateral actuators with left aileron stuck.

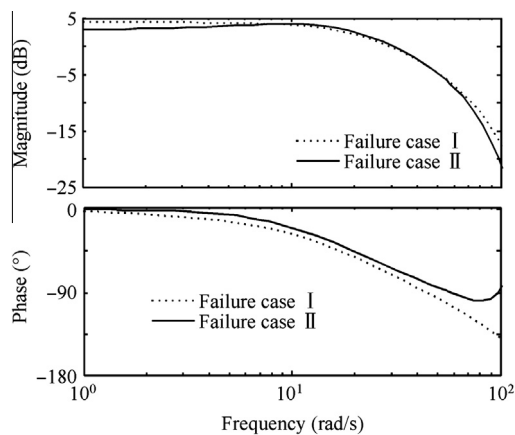


Fig. 13 Frequency responses of closed-loop dynamic control allocation in two failure cases in longitudinal direction.

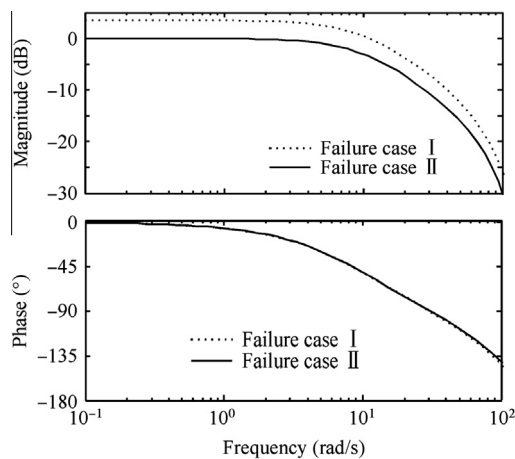


Fig. 14 Frequency responses of closed-loop dynamic control allocation in two failure cases in lateral direction.

counteract the disturbance from the roll channel. And the eigenvalues of  $V_u(k)$  are  $\lambda_1^u = 1$  and  $\lambda_2^u = 0.5$ , and  $u(\infty) = [10^\circ \ 10^\circ \ -0.005^\circ \ -0.005^\circ]^\top$ . According to Corollary 2, the closed-loop dynamic control allocation system is stable. The actuator deflections in Fig. 12 are very close to the  $u(\infty)$  when the simulation time extends to 80 s.

Figs. 13 and 14 show the open-loop frequency responses of closed-loop dynamic control allocation system in two cases in both longitudinal and lateral directions. We can see the proposed method has enough gain and phase margins before losing stability.

## 5. Conclusions

In this paper, a closed-loop control allocation approach is proposed for aircraft with multiple actuators. By combining closed-loop configuration with dynamic control allocation, the proposed method guarantees that the closed-loop system is stable in the absence or presence of actuator failures, and the actuators work in their respective frequency domains. The CRW aircraft model example demonstrates the effectiveness of the proposed approach.

The actuator dynamics presented here do not contain actuator saturation. Therefore, the closed-loop dynamic control allocation approach with actuator saturation is our future research.

## Acknowledgement

This study was supported by Program for New Century Excellent Talents in University (NCET-10-0032).

## References

1. Snell SA, Enns DF, Garrard WL. Nonlinear inversion flight control for a supermaneuverable aircraft. *J Guid Control Dyn* 1992;**15**(4):976–86.
2. Enomoto K, Yamasaki T, Takano H, Baba Y. Guidance and control system design for chase UAV; 2008. Report No.: AIAA-2008-6842.
3. Ezal K, Pan Z, Kokotović PV. Locally optimal and robust backstepping design. *IEEE Trans Autom Control* 2000;**45**(2):260–70.
4. Sonneveldt L, Chu QP, Mulder JA. Nonlinear flight control design using adaptive backstepping. *J Guid Control Dyn* 2007;**30**(2):322–36.
5. Bodson M. Evaluation of optimization methods for control allocation. *J Guid Control Dyn* 2002;**25**(4):703–11.
6. Shtessel YB, Buffington JM, Banda SS. Tailless aircraft flight control using multiple time scale reconfigurable sliding modes. *IEEE Trans Control Syst Technol* 2002;**10**(2):288–96.
7. Durham WC. Constrained control allocation. *J Guid Control Dyn* 1993;**16**(4):717–25.
8. Tang SY, Zhang SJ, Zhang YL. A modified direct allocation algorithm with application to redundant actuators. *Chin J Aeronaut* 2011;**24**(3):299–308.
9. Buffington JM, Enns DF. Lyapunov stability analysis of daisy chain control allocation. *J Guid Control Dyn* 1996;**19**(6):1226–30.
10. Petersen JAM, Bodson M. Constrained quadratic programming techniques for control allocation. *IEEE Trans Control Syst Technol* 2006;**14**(1):91–8.

11. Poonamallee VL, Yurkovich S, Serrani A, Doman DB. A nonlinear programming approach for control allocation. In: *Proceedings of the 2004 American control conference*; 2004. p. 1689–94.
12. Härkegård O. Dynamic control allocation using constrained quadratic programming. *J Guid Control Dyn* 2004;**27**(6):1028–34.
13. Arun Kishore WC, Sen S, Ray G, Ghoshal TK. Dynamic control allocation for tracking time-varying control demand. *J Guid Control Dyn* 2008;**31**(4):1150–7.
14. Yang LY, Fan YM, Shao S, Zhong YW, Shen GZ. Flight control based on the moment compensation and control allocation for aircraft with multiple control effectors. *Control Theory Appl* 2010;**27**(5):631–5 [Chinese].
15. Stevens BL, Lewis FL. *Aircraft control and simulation*. New York: John Wiley & Sons; 2003.
16. Durham WC, Bordignon KA. Multiple control effector rate limiting. *J Guid Control Dyn* 1996;**19**(1):30–7.
17. Gai WD, Wang HL, Li DW. Flight dynamic modeling and analysis for the canard rotor/wing UAV. *Acta Aerodyn Sin* 2012;**30**(2):244–9 [Chinese].
18. Gai WD, Wang HL, Guo TF, Li DW. Modeling and LPV flight control of the canard rotor/wing unmanned aerial vehicles. In: *Proceedings of second international conference on artificial intelligence, management science and electronic commerce*; 2011. p. 2187–91.
19. Bass SM, Thompson TL, Rutherford JW, Swanson S. Low-speed wind tunnel test results of the canard rotor/wing concept; 1993. Report No.: AIAA-1993-3412.
20. Mitchell CA, Vogel BJ. The canard rotor wing (CRW) aircraft: a new way to fly; 2003. Report No.: AIAA-2003-2517.

**Gai Wendong** received his B.S. and M.S. degrees in automatic control from Shandong University of Science and Technology, China, in 2005 and 2008, respectively. He is currently a Ph.D. candidate in navigation, guidance and control, Beihang University (BUAA). His research interests include modeling and nonlinear flight control of unmanned aerial vehicles, adaptive control of nonlinear systems, and the application of advanced control and optimization techniques to aerospace.

**Wang Honglun** received the B.S., M.S., and Ph.D. degrees in fire control from Northwestern Polytechnical University, China, in 1992, 1995 and 1998, respectively. From 1998 to 2000, he did his postdoctoral research at Nanjing University of Aeronautics and Astronautics, China. In 2000, he joined the Unmanned Aerial Vehicle Research Institute, Beihang University (BUAA), as an associate professor. Since 2004, he has been a professor affiliated with navigation, guidance and control, BUAA. In 2009, he was chosen by the New Century Excellent Researcher Award Program from Ministry of Education of China. His research interests include autonomous flight control for unmanned aerial vehicles, sense and avoid technology for unmanned aerial vehicles, fire control, and automated aerial refueling.